Journal of Catalysis 282 (2011) 228–236

Contents lists available at ScienceDirect

Journal of Catalysis

journal homepage: www.elsevier.com/locate/jcat

Influence of the support composition and acidity on the catalytic properties of mesoporous SBA-15, Al-SBA-15, and Al_2O_3-supported Pt catalysts for cinnamaldehyde hydrogenation

Soraya Handjani [a,b], Eric Marceau [a,b,*], Juliette Blanchard [a,b], Jean-Marc Krafft [a,b], Michel Che [a,b,c], Päivi Mäki-Arvela [d], Narendra Kumar [d], Johan Wärnå [d], Dmitry Yu. Murzin [d]

[a] Laboratoire de Réactivité de Surface, UMR 7197 CNRS, Case 178, UPMC, 4 Place Jussieu, 75252 Paris Cedex 05, France
[b] CNRS, 4 Place Jussieu, 75252 Paris Cedex 05, France
[c] Institut Universitaire de France, France
[d] Laboratory of Industrial Chemistry and Reaction Engineering, Åbo Akademi, Biskopsgatan 8, 20500 Åbo, Finland

ARTICLE INFO

Article history:
Received 26 April 2011
Revised 14 June 2011
Accepted 16 June 2011
Available online 20 July 2011

Keywords:
Cinnamaldehyde hydrogenation
Selective hydrogenation
Acidity
Platinum
Mesoporous supports

ABSTRACT

Three Pt catalysts exhibiting similar metal particles size (<2 nm) were prepared on mesoporous supports differing by their chemical composition and tested in the liquid phase hydrogenation of cinnamaldehyde. The hydrogenation of the C=C bond was favored with Pt/SBA-15 and Pt/Al-SBA-15, with significantly higher reaction rates on the latter catalyst. The acidic support changes the adsorptive properties of the platinum nanoparticles, modifying their surface electron density and possibly their morphology. In contrast, Pt/Al_2O_3 was the most selective catalyst of the series toward cinnamyl alcohol, with C=C and C=O hydrogenations taking place at the same rate. The presence of Lewis acidic sites close to the particles is assumed to favor the adsorption of molecules via their polar C=O bond. Even if cinnamaldehyde hydrogenation does not require acidic sites to be performed, the composition and acidity of the support significantly influence the reaction rate and selectivity.

1. Introduction

The ever increasing demand for specialty chemicals has raised the selective hydrogenation of α,β-unsaturated aldehydes to one of the current challenges to be tackled both from the fundamental and from the industrial standpoints [1]. Within this family of reactions, the selective production of cinnamyl alcohol (C_6H_5—CH=CH—CH_2OH) from cinnamaldehyde (C_6H_5—CH=CH—CH=O) is highly sought for, because this unsaturated alcohol is an important additive in the food and pharmaceutical industries. Cinammyl alcohol has been synthesized through the Meerwein–Ponndorf–Verley reaction [2,3], with selectivities up to 85–90%, but this procedure also leads to the production of aluminum-containing by-products [4,5]. To overcome this problem, new and more direct reaction pathways involving noble metal-based heterogeneous catalysts have been investigated over the past years and reviewed [6,7].

The initial hydrogenation of cinnamaldehyde can yield two compounds: the unsaturated alcohol C_6H_5—CH=CH—CH_2OH and the saturated aldehyde C_6H_5—CH_2—CH_2—CH=O (Fig. 1). Because the hydrogenation of the C=C bond is thermodynamically favored and the desorption of the alcohol is slower [8], the major product is usually the saturated aldehyde. However, the selectivity to cinnamyl alcohol has been found to be highly dependent on the catalyst composition and structure. The catalytic properties of the systems described in the literature are influenced by three main parameters:

(i) the adjunction of promoters to the catalysts, such as a second metal (Fe, Ge, Sn, Ga) [7,9–11] or, in zeolites, a promoter of basicity (Ba, Sr) [12], which tunes the catalytic properties of the system with excellent results in terms of selectivity.
(ii) the size of the metal particles. Larger, faceted Pt or Ru particles would favor the adsorption of cinnamaldehyde via its C=O bond and thus the production of cinnamyl alcohol [13,14]. However, a reverse effect was observed with Au catalysts, on which smaller particles (1 nm) were more selective [15]. An enhanced back donation between the C=O bond and the electron-enriched surface of the Au nanoparticles has been invoked to explain this observation.
(iii) the nature of the support. On non-silicoaluminic supports, SMSI effects [16,17] or variations of the support hydrophilicity [18,19] have been shown to influence the catalyst properties.

* Corresponding author at: Laboratoire de Réactivité de Surface, UMR 7197 CNRS, Case 178, UPMC, 4 Place Jussieu, 75252 Paris Cedex 05, France. Fax: +33 1 44 27 60 33.
E-mail address: eric.marceau@upmc.fr (E. Marceau).

0021-9517/$ - see front matter © 2011 Elsevier Inc. All rights reserved.
doi:10.1016/j.jcat.2011.06.017

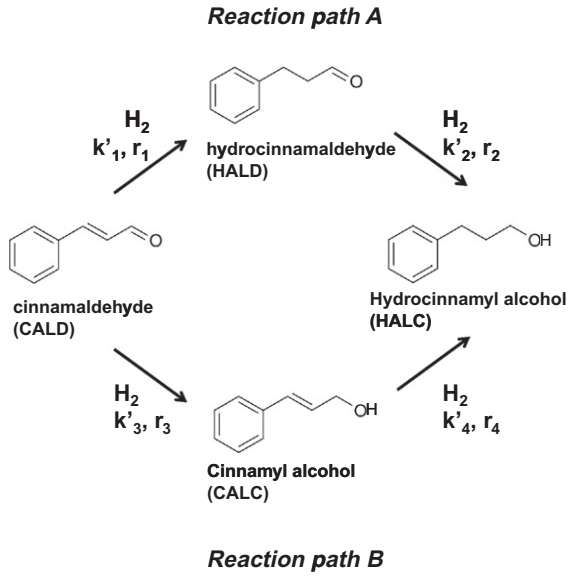

Fig. 1. Reaction pathways and definition of the rate constants in the catalytic hydrogenation of cinnamaldehyde.

On silicoaluminic supports, high selectivities have been reported for Pt catalysts supported on zeolites Y and BEA [5,20].

The acidity or the basicity of the support is often put forward to explain these results, but with conflicting interpretations [5,12,14]. In fact, any rationalization is made difficult because modifications of the support (parameter (iii)) are often strongly correlated with the two other parameters: alkaline earth ions may have been introduced onto the support to change the catalyst properties (parameter (i) [12]); the metal dispersion may considerably change depending on the support nature, composition, and surface properties (parameter (ii) [4,21]). The influence of the support acid–base properties on a reaction that does not require acidic sites still remains puzzling.

In the present paper, we have attempted to consider this problem from a fundamental point of view and investigated how a change of the support composition and acidity would modify the catalytic properties of Pt-based systems whose structural characteristics (particles size, support porosity) would be as close as possible. The choice of mesoporous supports (SBA-15, Al-SBA-15, Al_2O_3), till now less studied than microporous ones [4,21,22], allowed us to prepare catalysts with different acidic surface properties and similar platinum dispersions. Catalytic results have been complemented by an infrared study of CO adsorption on the metal particles, which may provide some hints on the way each support influences the metal nanoparticles properties.

2. Experimental

2.1. Supports preparation

The synthesis of purely siliceous SBA-15 was carried out as reported in the literature, using TEOS (Fluka) as a precursor and block-copolymer Pluronic P123 (Aldrich) as a porogen [23]. The solid obtained after precipitation and aging, first at 38 °C under stirring (24 h) then at 95 °C in static conditions (72 h), was separated by filtration, washed several times with deionized water, dried at 95 °C for 16 h, and calcined (heating rate 1 °C min^{-1}) at 550 °C in a muffle furnace, with a plateau of 6 h at this temperature.

The alumination procedure of SBA-15 was realized following a postsynthesis method described in the literature [24,25]. Prior to grafting, the SBA-15 support was dehydrated at 450 °C for 2 h (heating rate 4 °C min^{-1}) and added to a solution of 3.18 g of aluminum isopropoxide (Aldrich) in 60 mL of dry cyclohexane (Fluka), under a flow of dry argon. The resulting suspension was left under stirring for 16 h. The final gel-like material was recovered by filtration and washed several times with cyclohexane. The resulting solid was then calcined at 500 °C (heating rate of 1 °C min^{-1}) with a plateau of 4 h at this temperature. A Si/Al atomic ratio of 6 was determined by chemical analysis performed using ICP at the Vernaison Center of Chemical Analysis of CNRS.

Because mesostructured aluminas may exhibit a poor stability upon introduction of the active phase in an aqueous solution [26], a non-mesostructured, mesoporous, and stable alumina was preferred to prepare the Pt/Al_2O_3 catalyst. The procedure has been initially described by Xu et al. [27] and later reviewed by Handjani et al. [28]. It involves an equimolar mixture of aluminum isopropoxide as a precursor and glucose as a porogen. After precipitation at pH 5 and standing at room temperature for 5 h, the milky mixture was heated at 100 °C in air to remove water and other volatile components, leading to a brown solid gel, which was calcined at 600 °C for 6 h (heating rate 1 °C min^{-1}) to completely remove the organic additive.

2.2. Catalysts preparation

Supported 1 wt.% Pt catalysts were prepared on SBA-15 and Al-SBA-15 according to an electrostatic adsorption method described earlier [25,29]. The Pt precursor was $Pt(NH_3)_4(OH)_2$. Two hundred microliter of the Pt solution (Alfa Aesar, 0.52 mol L^{-1}) was dissolved into 400 mL of deionized water. Two gram of the support was added to this solution whose pH was adjusted to 8 by dropwise addition of a 0.1 mol L^{-1} ammonia solution. The suspension was left under stirring for 3 h at room temperature. The solid was recovered by filtration, washed with deionized water and centrifuged three times, dried first at room temperature under vacuum for 16 h and under oxygen flow at 150 °C for 2 h afterward (flow rate 1 L min^{-1} g^{-1}, heating rate 1 °C min^{-1}). Platinum was then reduced under hydrogen flow at 500 °C for 2 h (flow rate 0.1 L min^{-1}, heating rate 2 °C min^{-1}). It was shown by CO adsorption followed by infrared spectroscopy that 500 °C was the lowest temperature allowing one to attain a complete reduction in Pt on Pt/SBA-15 (absence of CO/Pt^{x+} band above 2100 cm^{-1} at the lowest coverages).

Due to a poor electrostatic interaction between alumina and $[Pt(NH_3)_4]^{2+}$ at pH 8 and to the partial transformation of mesoporous alumina into $Al(OH)_3$ upon exposure to large amounts of water [28], platinum was deposited on Al_2O_3 by incipient wetness impregnation, using a 0.043 mol L^{-1} solution of $[Pt(NH_3)_4](OH)_2$ prepared from the commercial solution mentioned above. Because alumina exhibits a specific surface area lower than that of SBA-15 and Al-SBA-15, the Pt content was limited to 0.5 wt.% Pt, in order to prevent an increase in the particles size that might be consecutive to a poor distribution of Pt on the support. After one night of drying at 90 °C, the catalyst was reduced in a flow of H_2 at 400 °C for 2 h (flow rate 0.1 L min^{-1}, heating rate 2 °C min^{-1}). This temperature of reduction was chosen in order to obtain a Pt dispersion similar to that of Pt/SBA-15 and Pt/Al-SBA-15.

The three catalysts will be referred to as: Pt/SBA-15; Pt/Al-SBA-15; and Pt/Al_2O_3. Pt contents, Al content, and reduction temperatures will not be recalled.

2.3. Catalysts characterization

Elemental analysis for Pt was performed by ICP at the Vernaison Center of Chemical Analysis of CNRS. X-ray diffraction analyses

(XRD) were carried out at low angles on a Bruker D8 diffractometer, using Cu Kα radiation (0.15418 nm). Specific surface areas and pore characteristics of the catalysts were determined by the BET and BJH models from nitrogen adsorption/desorption experiments carried out at −196 °C on samples outgassed at 150 °C for 4 h prior to analysis, using an automatic Micromeritics ASAP 2010 M instrument. After reduction under a flow of 5% H_2/Ar and desorption of chemisorbed hydrogen in Ar at the temperature of reduction, platinum dispersion was measured at ambient temperature by H_2–O_2 titrations for Pt/SBA-15 and Pt/Al-SBA-15 (H/Pt_s=O/Pt_s = 1) and by CO chemisorption for Pt/Al_2O_3 (CO/Pt_s = 1), using an Autochem 2910 (Micromeritics).

Transmission Electron Micrographs (TEM) were collected on the reduced catalysts using a 200 kV JEOL JEM 2010 microscope. This instrument is equipped with a system for EDX analysis (IMIXPRISM detector) with an analysis domain of 100 nm. Ultramicrotomed slices (ca. 50 nm thick) were used to obtain extensive electron-transparent regions. The samples were prepared by embedding the material in a polymer resin subsequently cured at 70 °C for 2 days. Slices were cut using a diamond knife.

Transmission FTIR spectra of adsorbed CO were collected on a Bruker Vector 22 spectrometer using a DTGS detector (resolution 2 cm^{-1}, 64 scans per spectrum). The setup, described earlier [30], allows one to raise or lower the sample vertically between the two sections of the cell: the upper oven section in which thermal treatment takes place and the lower section equipped with a perpendicular body mounted with CaF_2 windows, cooled to liquid nitrogen temperature (LNT), where measurements take place. Dried samples were pressed into self-supported wafers of 15 mg and 1 cm^2. The wafer was first heated *in situ* at the temperature of reduction for 1 h under a flow of 5% H_2/Ar (flow rate 50 mL min^{-1}, heating rate 2 °C min^{-1}), before being outgassed (5×10^{-6} Torr) at the same temperature for 1 h. The wafer was then moved to the lower part of the cell, which was cooled down to ca. 100 K with liquid nitrogen. Pulses of CO were successively added (five pulses of 8.9×10^{-8} mol CO, followed by 13 pulses of 4.5×10^{-7} mol). The difference spectra were obtained by subtracting the spectrum of the dehydrated sample recorded at LNT from those recorded after successive increments in CO. In case of Pt/Al_2O_3, CO adsorption was carried out at room temperature after reduction and outgassing, because at LNT the CO/Pt band was not discernible due to the very intense bands resulting from the competitive adsorption of CO on the Al_2O_3 surface sites (Lewis sites, 2187 cm^{-1}; Al–OH sites, 2156 cm^{-1} [31]). At room temperature, only the CO/Pt bands were present.

2.4. Catalytic test

The catalysts were tested for the cinnamaldehyde hydrogenation reaction in a 500 mL stainless steel stirred semi-batch reactor (Autoclave Engineers, USA) equipped with a sample port, a reagent injection port, gas inlet, and vent, at $P(H_2)$ = 30 bar [10,18,19]. The prereduced catalyst samples (0.3–0.5 g, 25–90 μm) were activated *in situ* in H_2 (4 bar) at 350 °C for 2 h before transfer into the reactor filled with hydrogen. 160–310 mg cinnamaldehyde (98%, Aldrich) dissolved in 200 mL of 2-pentanol (Merck, p.a.) was then introduced into the autoclave. The reaction took place for 3 h at 95 °C (above 100 °C, cracking side reactions may be favored), under kinetic control (stirring rate: 1500 rpm). 2-Pentanol was chosen because as a polar solvent it increases the reaction rate, while its C_5 alkyl chain limits side reactions of acetalization compared to alcohols with shorter chain [21]. Aliquots of the reaction mixture (1–1.5 mL) were withdrawn periodically and analyzed on a gas chromatograph (GC Agilent 6890 N) equipped with autoinjector, FID detector, and Agilent DB-1 column. It should be noted that the initial time reported on the conversion curves corresponds to the first analysis time, 5–10 min after reactant and catalyst have been contacted. The hydrogenation of cinnamaldehyde (CALD) can result in hydrocinnamaldehyde (HALD), cinnamyl alcohol (CALC), and the fully hydrogenated hydrocinnamyl alcohol (HALC) (Fig. 1). Reaction pathway A leads to HALD and then HALC (hydrogenation of the C=C bond, then of the C=O bond); reaction pathway B leads to CALC and then to HALC (hydrogenation of the C=O bond, then of the C=C bond). The conversion of CALD and selectivity to CALC, HALD, and HALC were calculated as described before [19]. The kinetic experiments were modeled using the Odessa solver in the Modest 6.1 program package (Profmath Oy, Helsinki, 2002).

3. Results

3.1. Catalysts characterization

X-ray diffractograms of the catalysts are similar to those of the three pristine supports (not shown), confirming the preservation of the ordered mesoporosity of the SBA-15 and Al-SBA-15 systems (reflections (1 0 0), (1 1 0), and (2 0 0)) and of the γ-Al_2O_3 structure of the aluminic system.

The main structural and physicochemical characteristics of the three catalysts and corresponding supports are summarized in Table 1. The presence of a mesoporosity is evidenced by N_2 physisorption isotherms (not shown). The steep uptake of N_2 for Pt/SBA-15 and Pt/Al-SBA-15 indicates the presence of cylindrical mesopores whose diameter (6.2–6.5 nm) is identical to that of the corresponding support. For these two catalysts, the specific surface area decreases by about 15% compared with the supports, mostly due to a clogging of the microporosity upon platinum introduction. It was shown that the alumina BET specific surface area does not decrease when Pt is introduced by incipient wetness impregnation [28]. In contrast to the SBA-15 and Al-SBA-15 systems, the porosity of Pt/Al_2O_3 is intergranular and the shape of the hysteresis suggests an "ink-bottle" structure of the pores with smaller apertures. The diameter of the pores calculated from the adsorption branch of the isotherm was evaluated to be 5.6 nm [28].

Pt dispersion measurements led to similar results on the three catalysts: 62–69%, i.e., an average particle diameter of 1.6–1.8 nm, assuming that the particles are hemispherical. No particle larger than 2 nm was observed on TEM images of bulk

Table 1
Physicochemical characteristics of the three catalysts and their supports.

Support/ catalyst	BET specific surface area ($m^2 g^{-1}$)	Mesopore surface area ($m^2 g^{-1}$)	Micropore surface area ($m^2 g^{-1}$)	Mesopore diameter (nm)	Mesopore volume ($cm^3 g^{-1}$)	Pt dispersion (%)	Ø Pt particles (nm)
SBA-15	867	531	233	6.5	0.90	–	–
Pt/SBA-15	749	500	152	6.5	0.88	69	1.6
Al-SBA-15	525	342	94	6.3	0.57	–	–
Pt/Al-SBA-15	438	318	15	6.2	0.56	69	1.6
Al_2O_3	367	367	–	5.6	0.60	–	–
Pt/Al_2O_3	356	356	–	5.3	0.55	62	1.8

catalysts grains or of ultramicrotomed slices. Furthermore, for Pt/SBA-15 and Pt/Al-SBA-15, no Pt particle could be seen on the external surface of the ordered support. EDX analysis over 10 different support grains confirmed that the distribution of Pt over the three supports was homogeneous.

3.2. CO adsorption/IR spectroscopy

At LNT, CO is a molecule able to interact with cationic sites (Lewis acids) and perturb the proton of oxidic surface OH groups (Brønsted acids) by bonding via its carbon atom. Moreover, for a given type of site, the position of the perturbed ν(CO) band depends on the strength of the site: the stronger the acidic site, the higher the energy [25,31]. CO is also a well-known probe molecule for metallic sites, especially because the position of the CO band is sensitive to the particles electronic density. CO adsorption followed by infrared spectroscopy thus appears as a suitable technique to compare both the acidic properties of the supports and the adsorptive properties of the Pt nanoparticles. Spectra recorded on the three catalysts are presented in Fig. 2.

In terms of acidity, former results have shown that neither Pt/SBA-15 nor Pt/Al_2O_3 exhibits any acidic character toward two test reactions, cumene cracking and isopropanol dehydration [25]. For the Pt/SBA-15 sample, the only band related to the adsorption onto the support is CO/silanol groups (2157 cm^{-1}) (Fig. 2a). It is recalled here that at room temperature, the bands corresponding to CO/weak Lewis sites (2187–2192 cm^{-1}) and CO/aluminol groups (2156 cm^{-1}) are not present for Pt/Al_2O_3 (Fig. 2c).

In contrast, several types of acidic sites are revealed by CO adsorption on Pt/Al-SBA-15 (Fig. 2b). Their analysis has been detailed in Ref. [25]. Besides CO adsorbed on Al_2O_3-like weak Lewis sites (2196 cm^{-1}), present in low quantity, and on SiO_2-like silanol groups (2158 cm^{-1}), the spectra present bands typical of silica-aluminas and assigned to CO/strong Lewis sites (2230 cm^{-1}; isolated Td Al atoms) and CO/strong and medium Brønsted sites (2173 and 2168 cm^{-1}; presumably Si—OH···Al groups [32,33]). The latter are distinguished from Si—OH and Al—OH groups by their ability to crack cumene and dehydrate isopropanol into isopropene [25]. Pt/Al-SBA-15 is thus the only catalyst that exhibits strong Lewis and Brønsted acidities after thermal activation. Pt/Al_2O_3 exhibits a large number of weak Lewis acid sites, while Pt/SBA-15 exhibits only the very weak Brønsted acidity of silanols.

Two regions can be distinguished in the zone of the spectra corresponding to the CO/Pt band. An intense band between 2000 and 2100 cm^{-1} is assigned to CO linearly adsorbed on the Pt nanoparticles. At lower energies (1800–1900 cm^{-1}), one can find a broad and weak band attributed to bridging CO adsorbed on two Pt atoms. This mode of adsorption is usually favored on larger faceted particles. The low intensity of this band confirms that facets are scarce on the nanoparticles of the three catalysts, in line with the high dispersion measured by chemisorption. Beside this, it has also been reported that the quantity of bridging CO/Pt is low for supports presenting poor basic properties [34,35], which is the case here.

As can be seen on Fig. 2, the position of the two CO/Pt bands varies depending on the support. A zoom on the region of linear CO/Pt is presented in Fig. 3 at iso-coverage, after adsorption of the first pulses of CO on Pt/SBA-15 and Pt/Al-SBA-15. Due to competitive adsorption on strong Lewis and Brønsted acidic sites, CO coverage of nanoparticles is smaller on Pt/Al-SBA-15 than on Pt/SBA-15 for the same amount of CO introduced; the number of pulsed required to reach the same coverage of the metallic sites is therefore larger on Pt/Al-SBA-15. The position of the CO/Pt band does not change with coverage for Pt/SBA-15 (ν(CO/Pt) = 2079 cm^{-1}), whereas for Pt/Al-SBA-15 it shifts by about +2 cm^{-1} between pulse 3 and pulse 7 and remains at the same position for the next CO pulses (2086 cm^{-1}). The difference between the two catalysts in terms of band position is significant and reproducible and larger than the initial coverage-related shift detected on Pt/Al-SBA-15. Finally, the position of the band does not change after heating to room temperature.

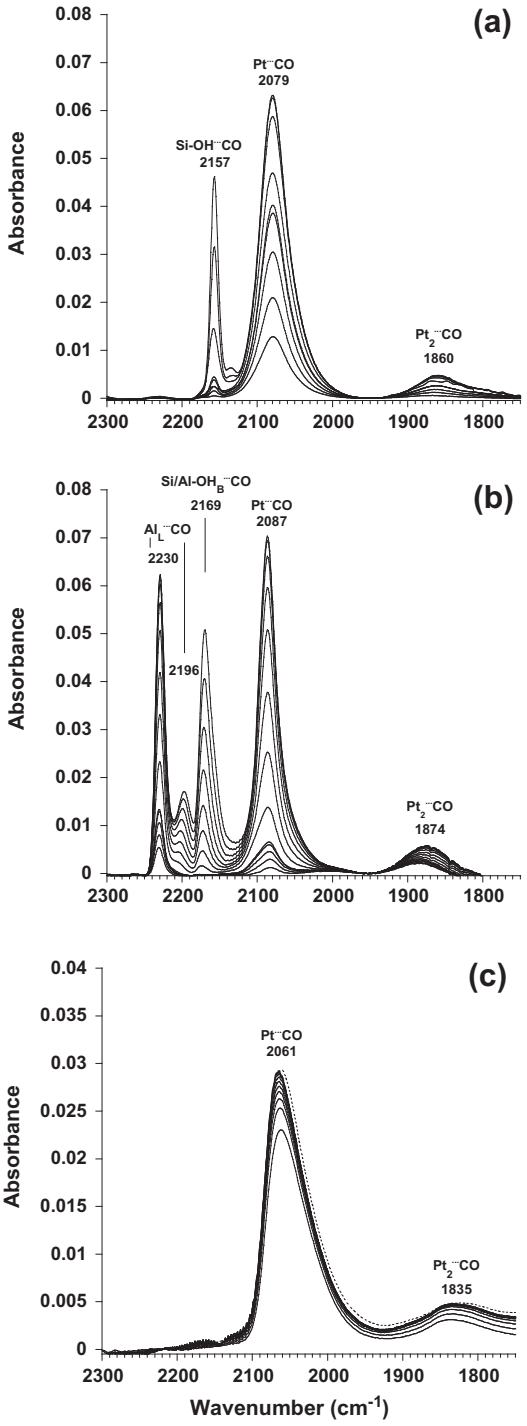

Fig. 2. FTIR spectra of: (a) Pt/SBA-15; (b) Pt/Al-SBA-15; and (c) Pt/Al_2O_3, after successive introductions of CO pulses. Recording of the spectra was carried out at LNT for Pt/SBA-15 and Pt/Al-SBA-15 and at ambient temperature for Pt/Al_2O_3, except for the spectrum in dotted lines recorded after cooling down to LNT. For Pt/Al-SBA-15, the drift of the baseline in the 1850–1950 cm^{-1} region, seen from the first pulse, results from the initial subtraction of the spectra.

The highest position in energy of ν(CO/Pt) is thus observed for Pt/Al-SBA-15, while for Pt/SBA-15 the band looks broader with possibly high- and low-energy contributions (Fig. 2a and b,

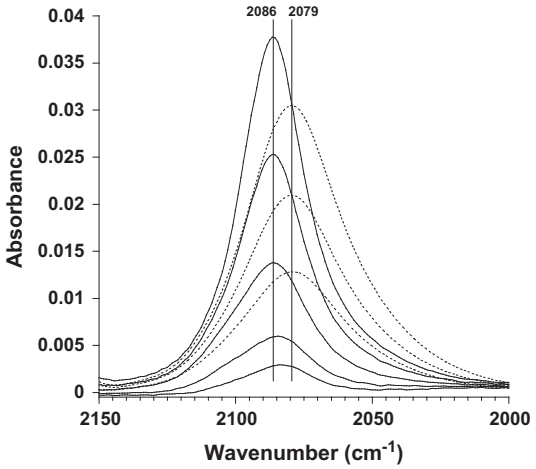

Fig. 3. Zoom on the linear CO/Pt region for Pt/Al-SBA-15 (full lines, pulses 3, 5, 7, 8, and 9) and Pt/SBA-15 (dotted lines, pulses 1, 2, and 3).

Fig. 3). Despite similar dispersions, Pt nanoparticles on Pt/SBA-15 and Pt/Al-SBA-15 present different adsorptive properties, with a globally lower back-donation toward CO when particles are located on the more acidic support.

The position of the linear CO/Pt band on Pt/Al_2O_3 is located at a lower energy than the two others, 2061 cm^{-1} (Fig. 2c). We would like to remind here that at room temperature, the surface sites of the alumina support do not compete with Pt for CO adsorption. Consequently, the coverage of the Pt nanoparticles is high from the first CO pulse. Therefore, the position of the bands cannot be compared at iso-coverage with the two other catalysts. We will assume that for Pt/Al_2O_3 the position of the band does not change significantly with coverage as was observed for Pt/SBA-15 and Pt/Al-SBA-15. Concerning an effect of the temperature, we checked that the position of the band associated with CO linearly adsorbed on Pt was not modified after outgassing and decreasing the temperature of the cell to LNT. We can therefore conclude that the adsorptive properties of Pt nanoparticles also vary when the support is neither silica nor silica–alumina, but alumina.

Finally, the position of the bridging CO/Pt band follows the same trend as the linear CO/Pt band, with even larger shifts. Pt/Al-SBA-15 presents the band at the highest energy (1874 cm^{-1}), followed by Pt/SBA-15 (1860 cm^{-1}) and Pt/Al_2O_3 (1835 cm^{-1}).

3.3. Catalytic results

Conversion curves of cinnamaldehyde vs. time and selectivity plots vs. conversion are given in Figs. 4 and 5 respectively, while the parameters of each test are presented in Table 2. Unlike what has been observed during a test experiment on 1 wt.% Pt/H-beta catalyst (Si/Al = 75), no product of cracking or acetalization reaction was detected for any of the three catalysts. This shows that the Brønsted acidity of Pt/Al-SBA-15 is not as strong as that of a protonic zeolite. This type of mesoporous system is thus suitable to catalyze a reaction of selective hydrogenation without causing side reactions.

Reaction has started between the moment when the mixing and heating of catalyst and reactants starts and the first analysis, which explains why curves shown in Fig. 4 do not start at a molar fraction of 1 in CALD.

On Pt/SBA-15, the main product of reaction is HALD, resulting from the hydrogenation of the C=C bond. After 3 h of reaction, the conversion of CALD is not complete and a plateau seems to be reached in the production of HALD. The fully hydrogenated HALC comes second, with a selectivity increasing with time and

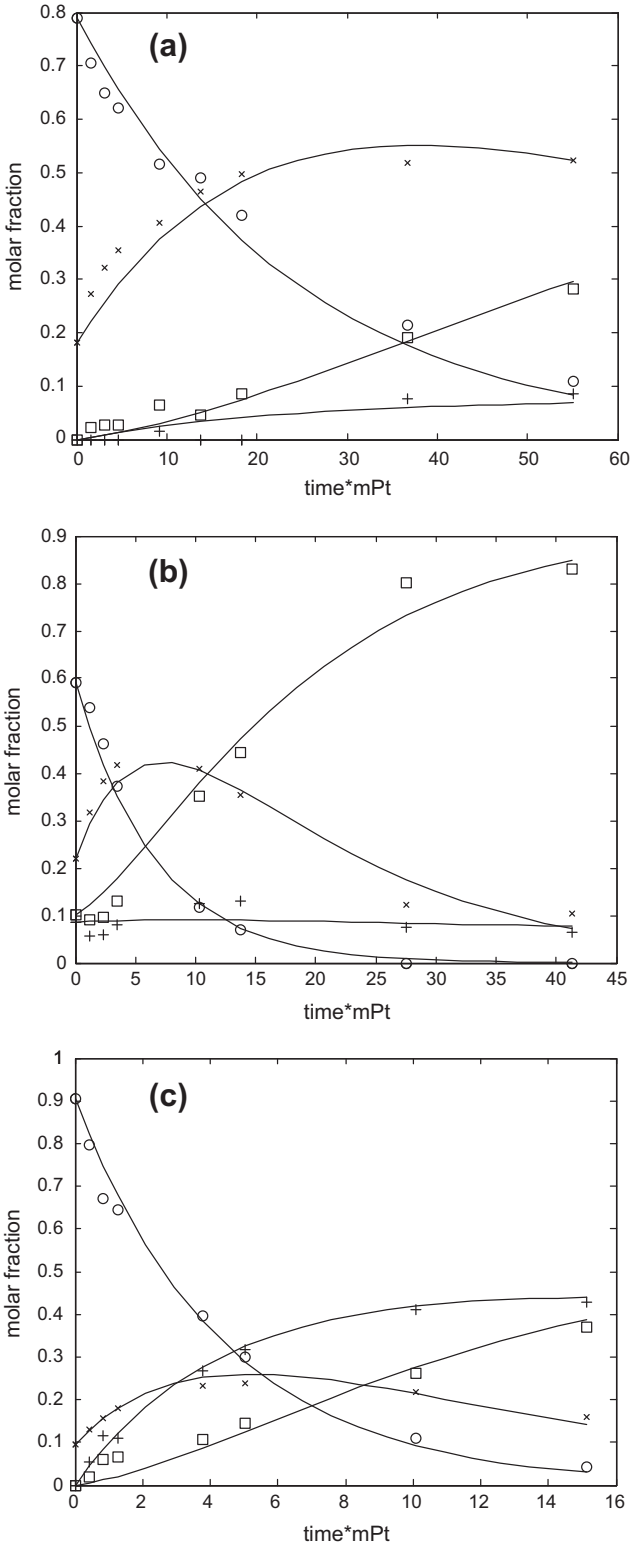

Fig. 4. Cinnamaldehyde conversion and product distribution as a function of time for: (a) Pt/SBA-15; (b) Pt/Al-SBA-15; and (c) Pt/Al_2O_3. O: CALD; x: HALD; □: HALC; +: CALC.

conversion. Cinnamyl alcohol (CALC), whose production tends to slowly increase with time, is a minor product on this catalyst (less than 10% of selectivity at 70% of conversion and after 3 h). Similar results have been reported for Pt particles supported on commercial silica [11].

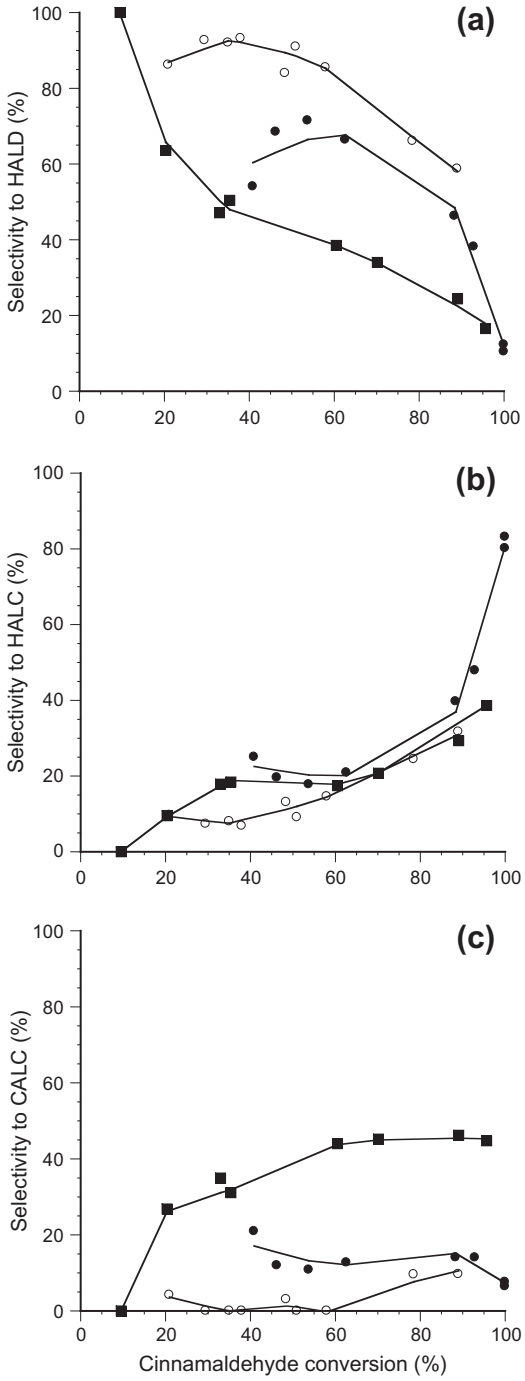

Fig. 5. Selectivity plots as a function of conversion. Open circles, Pt/SBA-15; full circles, Pt/Al-SBA-15; full squares, Pt/Al_2O_3.

Compared with the siliceous system, Pt/Al-SBA-15 exhibits a much higher activity, as evidenced by the higher conversion of CALD measured during the first analysis and by the completion of the reaction after 2 h only. During the first 50 min, HALD remains the major product of hydrogenation, indicating that the hydrogenation of the C=C bond is favored. But the conversion profile differs from that of Pt/SBA-15, since the production of HALD starts decreasing after 50 min and its selectivity drops sharply, while the production of HALC, initially low, constantly increases till reaching 80% of selectivity after 3 h. The S shape of the HALC curve suggests that HALD is an intermediate product, ultimately leading to HALC by hydrogenation of the C=O bond in agreement with pathway A of the reaction mechanism (Fig. 1). On Pt/Al-SBA-15 as well, CALC is the minor product, with a selectivity of 11% at 70% of conversion and a final selectivity of 8% after 3 h. Selectivity in CALC is almost constant with increasing conversion.

Compared with the two other systems, Pt/Al_2O_3 stands out in terms of selectivity. Conversion of CALD is almost complete after 3 h of reaction, despite the fact that the Pt content of the catalyst is lower than that of the two other systems (0.5 wt.% compared with 1 wt.%, Table 2). If initially the main product of reaction is HALD, the trend changes after 15 min for two reasons: (i) the production of HALC starts increasing constantly following reaction pathway A, and the maximum in HALD production at about 60 min shows that on this catalyst as well, HALD is an intermediate compound consumed by hydrogenation of its C=O bond; (ii) the production of CALC increases progressively following reaction pathway B. After 50 min of reaction, CALC is the main product of reaction and will remain so till the end of the run (46% of selectivity at 70% of conversion and after 3 h of reaction). Without a kinetic analysis of the curves, it is difficult to assert whether the hydrogenation of the C=C bond in CALC also contributes to the production of HALC. However, no maximum in the production of CALC is seen during the course of the reaction, unlike what is observed for HALD; the C=O reduction in HALD is probably faster that the C=C hydrogenation in CALC.

We have aimed at extracting apparent kinetic constants from these experimental curves. Data were fitted following the model developed for the most hydrophilic Pt/carbon nanofibers catalyst described by Toebes et al. [18]. According to this model: (i) the reaction proceeds through a Langmuir–Hinshelwood mechanism; (ii) no competition takes place with hydrogen and dissociative hydrogen adsorption is assumed.

The rate equations (notation is given in Fig. 1) then take the following form

$$r_1 = \frac{k_1 \cdot c_{CALD} \cdot K_{CALD}}{(1 + c_{CALD} \cdot K_{CALD} + c_{HALD} \cdot K_{HALD} + c_{CALC} \cdot K_{CALC} + c_{HALC} \cdot K_{HALC})} \cdot \frac{\sqrt{c_{H_2} \cdot K_H}}{1 + \sqrt{c_{H_2} \cdot K_H}} \quad (1)$$

$$r_2 = \frac{k_2 \cdot c_{HALD} \cdot K_{HALD}}{(1 + c_{CALD} \cdot K_{CALD} + c_{HALD} \cdot K_{HALD} + c_{CALC} \cdot K_{CALC} + c_{HALC} \cdot K_{HALC})} \cdot \frac{\sqrt{c_{H_2} \cdot K_H}}{1 + \sqrt{c_{H_2} \cdot K_H}} \quad (2)$$

$$r_3 = \frac{k_3 \cdot c_{CALD} \cdot K_{CALD}}{(1 + c_{CALD} \cdot K_{CALD} + c_{HALD} \cdot K_{HALD} + c_{CALC} \cdot K_{CALC} + c_{HALC} \cdot K_{HALC})} \cdot \frac{\sqrt{c_{H_2} \cdot K_H}}{1 + \sqrt{c_{H_2} \cdot K_H}} \quad (3)$$

Table 2
Experimental parameters for the catalytic tests in cinnamaldehyde hydrogenation.

Catalyst	Pt wt.%	Pt dispersion (%)	Amount of catalyst (g)	Amount of cinnamaldehyde (g)	Concentration in cinnamaldehyde (mol L^{-1})	Molar ratio cinnamaldehyde/Pt_s
Pt/SBA-15	1.0	69	0.510	0.307	11×10^{-3}	129
Pt/Al-SBA-15	1.0	69	0.383	0.228	8×10^{-3}	142
Pt/Al_2O_3	0.5	62	0.280	0.168	6×10^{-3}	285

Table 3
Apparent kinetic constants k'_1 ($\times 10^3$ min^{-1}) extracted from the fits of the curves presented in Fig. 4 (inside brackets: estimation of the 95% confidence interval).

	Reaction pathway A		Reaction pathway B	
	k'_1 CALD → HALD (C=C)	k'_2 HALD → HALC (C=O)	k'_3 CALD → CALC (C=O)	k'_4 CALC → HALC (C=C)
Pt/SBA-15	12 (9–15)	1 (0–2)	3 (2–4)	0
Pt/Al-SBA-15	34 (31–37)	1 (0–2)	16 (14–18)	2 (0–4)
Pt/Al_2O_3	8 (7–9)	10 (9–11)	9 (8–10)	1 (0–2)

$$r_4 = \frac{k_4 \cdot c_{CALC} \cdot K_{CALC}}{(1 + c_{CALD} \cdot K_{CALD} + c_{HALD} \cdot K_{HALD} + c_{CALC} \cdot K_{CALC} + c_{HALC} \cdot K_{HALC})} \cdot \frac{\sqrt{c_{H_2} \cdot K_H}}{1 + \sqrt{c_{H_2} \cdot K_H}} \quad (4)$$

Several simplifications can be introduced in these kinetic equations. At high H_2 pressure, the order associated with H_2 is zero. Moreover, preliminary modeling indicated that the reaction orders in each organic molecule in the four reactions listed in Fig. 1 are close to unity; thus, terms containing adsorption constants in the denominators of Eqs. (1)–(4) could be neglected leading finally to:

$$r_1 = k_1 \cdot c_{CALD} \cdot K_{CALD} = k'_1 \cdot c_{CALD}; r_2 = k_2 \cdot c_{HALD} \cdot K_{HALD} = k'_2 \cdot c_{HALD}$$
$$r_3 = k_3 \cdot c_{CALD} \cdot K_{CALD} = k'_3 \cdot c_{CALD}; r_4 = k_4 \cdot c_{CALC} \cdot K_{CALC} = k'_4 \cdot c_{CALC} \quad (5)$$

It should be noted that both on hydrophobic supports attracting the π ring of cinnamaldehyde [18,19] and for very high cinnamaldehyde/Pt_s ratios [36], the inhibiting contribution of cinnamaldehyde should be taken into account, e.g., the term $c_{CALD} \cdot K_{CALD}$ should be included in denominators of Eqs. (1)–(4). In contrast, molar ratios (cinnamaldehyde/surface Pt atoms) are close in the present work and in the work by Toebes et al. (129–285 in this work, 74–300 for an initial concentration in CALD of 14–34 10^{-3} mol L^{-1} in [18]). Four kinetic constants (labeled k'_1 to k'_4) are consequently obtained from the fits. Values are presented in Table 3.

The apparent rate constants increase considerably between Pt/SBA-15 and Pt/Al-SBA-15, i.e., the two catalysts on which reaction pathway A is the major path. The acidic catalyst displays the highest values of the series for k'_1 and k'_3, with k'_1 much larger than k'_3, in agreement with the experimental measurements of selectivities. By comparison, the kinetic constants associated with the secondary reactions are quite low. Pt/Al_2O_3 differs from the two other catalysts in two aspects: (i) constants k'_1 and k'_3 have similar values, in line with the selectivities in HALD and CALC up to 40 min of reaction; (ii) constant k'_2 corresponding to the reduction in the C=O bond in HALD is almost equal to k'_3, corresponding to the reduction in the C=O bond in CALD. On this catalyst, the hydrogenation of the C=O bond proceeds at the same rate whatever the organic substrate. In contrast, k'_4 (hydrogenation of the C=C bond in cinnamyl alcohol) remains very low.

4. Discussion

The results presented earlier show that the hydrogenation of cinnamaldehyde takes place differently on Pt catalysts prepared on mesoporous acidic supports, compared with non-acidic SBA-15 that we will consider as the reference system. Since the characteristics of the catalysts are very close in terms of porosity and Pt dispersion, the differences in catalytic behavior should be attributed to the effect of the support composition and/or acidity, though, apparently, cinnamaldehyde hydrogenation does not require acidic sites to be performed.

X-ray absorption and infrared spectroscopies correlated with catalytic data have provided some insight into the way supports can influence the properties of metal nanoparticles of small size (<2 nm) [34,37–39]. CO adsorption results detailed by Koningsberger's group on various types of Pt catalysts are in excellent agreement with our results, whether in terms of respective positions of the bands (at lower energy both for linear and bridging CO/Pt on Pt/Al_2O_3 [39]) or in terms of shifts toward higher energies when the acidity of the support increases [34]. Concurrently, activities in hydrogenation and hydrogenolysis reactions increase when the acidity of the support increases [38,39]. On a more acidic support, i.e., on a support containing oxygen atoms whose formal negative charge (or ionic character) is low, the electron density of the Pt nanoparticles is driven toward the metal – support interface. The electron density at the surface of the metal and thus electron back-donation toward adsorbates decrease [37,39], leading to less strongly adsorbed molecules [39]. This results in a higher activity of the acidic catalysts in reactions involving hydrogen. This model applies well to two of our catalysts. On both Pt/SBA-15 and Pt/Al-SBA-15, the hydrogenation of the C=C bond is favored, as commonly observed for Pt catalysts, but the rate of the reactions is significantly higher when the support is acidic.

It should be noted that some structural differences have been observed on Pt particles dispersed on acidic, non-acidic, or basic supports. Pt particles have been reported to flatten over the surface of acidic supports, as a way to increase the interaction between surface oxygens and metal atoms [34,39]. These changes are small and detected by X-ray absorption spectroscopy only. A difference in the particles morphology cannot be ruled out on our systems, as suggested by the broader bands for linear CO/Pt seen on Pt/SBA-15, which may correspond to the presence of several contributions instead of one on Pt/Al-SBA-15.

In contrast, it is the selectivity of the reaction that is completely modified in case of Al_2O_3 compared to SBA-15. Kinetically speaking, all the steps involving the hydrogenation of the C=O bond are on a par with that involving the initial hydrogenation of the C=C bond. Four main differences exist between Pt/Al_2O_3 and Pt/SBA-15:

(i) the presence of smaller pore apertures in alumina. However, cinnamaldehyde, a rigid molecule, has been shown to diffuse in micropores as well as mesopores [14].
(ii) a slightly lower dispersion. Cinnamaldehyde hydrogenation is a reaction sensitive to the particles size [40]. However, except in case of gold catalysts [15], the literature usually concludes that no significant effect of the particles size is expected on cinnamaldehyde hydrogenation in the 1–2 nm range [17].
(iii) the energy of the CO/Pt band, which is lower in case of Pt/Al_2O_3, denoting a more important back donation from the metal toward the adsorbates. This observation can be explained assuming either:
- specific morphologies for the Pt particles. Hydrogenation of the C=O bond is considered to be favored on particles facets, which repel the electron-rich aromatic ring and C=C bond of the molecule [41–43]. However, the ratio between the quantities of linear CO and bridging CO is

about the same for Pt/Al_2O_3 and Pt/SBA-15, making it difficult to sustain that particles would be considerably more faceted on the former.

- or a perturbation of the Pt nanoparticles by the support underneath. A higher selectivity in cinnamyl alcohol has been reported on particles whose surface was enriched in electrons, most often on basic supports [12,44]. An increase in the particles surface electron density is evidenced here by the stronger interaction of CO with the metal. One might infer that this favors the desorption of molecules adsorbed via the electron-rich —OH function, considered to be the rate-determining step for the production of alcohols [8].

(iv) the presence of numerous weak Lewis sites all over the support, including in the vicinity of the Pt nanoparticles, which would be involved in the adsorption of CALD and HALD via their polar C=O function [29,45]. This hypothesis has been also proposed in the literature to account for the selectivity of catalysts presenting a SMSI effect (partial covering of the metallic surface by oxidic species [16,17]) or by a second metallic element in an ionic state such as tin [10]. If this hypothesis is correct, the activity of a Pt catalyst can be strongly modified by a direct intervention of the support acidic groups, here Lewis sites acting on the adsorption of the organic substrates.

It can be noted that the selectivity in CALC measured on our Pt/Al_2O_3 catalyst is quite unexpected, when compared to results previously published by other groups on alumina-supported systems. Actually, with respect to cinnamaldehyde hydrogenation, Pt/Al_2O_3 catalysts reported in the literature can be divided into two categories as follows: catalysts that are selective in CALC because Pt particles are large and faceted (4–13 nm) [41,46]; catalysts on which Pt particles are well dispersed and behave poorly in CALC production [47,48]. In this latter category, one can observe that the aluminas employed are well crystallized, since their specific surface area is low (100–130 $m^2\ g^{-1}$), and presumably exhibit a low surface density of Lewis sites. This observation leads us to favor an explanation based on the action of Lewis sites, rather than on the enhanced surface electron density of Pt nanoparticles. The benefit of using a mesoporous alumina as a support would thus be dual: increasing the catalyst activity by bringing a high specific surface area and thus promoting a high dispersion of Pt nanoparticles and increasing the catalyst selectivity in CALC by supplying Lewis acid sites that favor the adsorption of CALD via the aldehyde function.

5. Conclusions

In the present paper, three Pt catalysts exhibiting similar pore size and metal dispersion, but prepared on mesoporous supports differing by their chemical composition and acidic properties, were tested in the liquid phase hydrogenation of cinnamaldehyde in 2-pentanol. When cinnamaldehyde hydrogenation is performed on Pt catalysts exhibiting particles size smaller than 2 nm, the support can influence the catalytic properties of the system in two ways:

(i) by modifying the electronic properties of the nanoparticles or perhaps their morphology. This is evidenced for mesoporous silicoaluminic supports exhibiting Brønsted and Lewis acidities (Al-SBA-15), on which Pt particles display a lower surface electron density than their homologs on siliceous SBA-15. In both cases, the hydrogenation of the C=C bond is favored, but rate constants increase dramatically when Al is introduced on the support. On Al-SBA-15, the major final product of reaction is the saturated alcohol.

(ii) by providing adsorption sites to the organic substrates, allowing them to interact with the catalyst via their polar C=O bond, as suggested for the Lewis sites on the surface of Al_2O_3. An enrichment of the particles surface electron density, deriving from the ionic character of alumina, might also favor the production of alcohols. Consequently, on alumina, the hydrogenation of cinnamaldehyde occurs through two parallel reaction pathways at the same rate, yielding cinnamyl alcohol on the one hand and C—C saturated molecules on the other hand.

Although cinnamaldehyde hydrogenation does not require acidic sites, the composition and acidity of the oxidic support can thus significantly influence the reaction rate or the selectivity of the process when Pt nanoparticles are small enough.

Acknowledgments

This work was part of the project Nanocat (No. 506621) funded through the European 6th Framework Program. The authors express their gratitude to Patricia Beaunier for her help in TEM measurements.

References

[1] G. Neri, L. Bonaccorsi, L. Mercadante, S. Galvagno, Ind. Eng. Chem. Res. 36 (1997) 3554.
[2] Y. Zhu, G.K. Chuah, S. Jaenicke, J. Catal. 241 (2006) 25.
[3] G.K. Chuah, S. Jaenicke, Y.Z. Zhu, S.H. Liu, Curr. Org. Chem. 10 (2006) 1639.
[4] J. Hájek, N. Kumar, P. Mäki-Arvela, T. Salmi, D.Yu. Murzin, I. Paseka, T. Heikkilä, E. Laine, P. Laukkanen, J. Väyrynen, Appl. Catal. A 251 (2003) 385.
[5] J. Hájek, N. Kumar, T. Salmi, D.Yu. Murzin, Catal. Today 100 (2005) 349.
[6] P. Gallezot, D. Richard, Catal. Rev. Sci. Eng. 40 (1998) 81.
[7] P. Mäki-Arvela, J. Hájek, T. Salmi, D.Yu. Murzin, Appl. Catal. A 292 (2005) 1.
[8] D. Loffreda, F. Delbecq, F. Vigné, P. Sautet, J. Am. Chem. Soc. 128 (2006) 1316.
[9] S. Galvagno, A. Donato, G. Neri, R. Pietropaolo, D. Pietropaolo, J. Mol. Catal. A 49 (1989) 223.
[10] A.J. Plomp, D.M.P. van Asten, A.M.J. van der Eerden, P. Mäki-Arvela, D.Yu. Murzin, K.P. de Jong, J.H. Bitter, J. Catal. 263 (2009) 146.
[11] J.M. Ramallo-López, G.F. Santori, L. Giovanetti, M.L. Casella, O.S. Ferretti, F.G. Requejo, J. Phys. Chem. B 107 (2003) 11441.
[12] G. Li, T. Li, Y. Xu, Chem. Commun. (1996) 497.
[13] L. Mercadante, G. Neri, C. Milone, A. Donato, S. Galvagno, J. Mol. Catal. A 105 (1996) 93.
[14] M. Lashdaf, V.V. Nieminen, M. Tiita, T. Venäläinen, H. Österholm, O. Krause, Micropor. Mesopor. Mater. 75 (2004) 159.
[15] E. Bus, R. Prins, J.A. van Bokhoven, Catal. Commun. 8 (2007) 1397.
[16] A.B. Boffa, C. Lin, A.T. Bell, G.A. Somorjai, Catal. Lett. 27 (1994) 243.
[17] M. Englisch, A. Jentys, J.A. Lercher, J. Catal. 166 (1997) 25.
[18] M.L. Toebes, T.A. Nijhuis, J. Hájek, J.H. Bitter, A.J. van Dillen, D.Yu. Murzin, K.P. de Jong, Chem. Eng. Sci. 60 (2005) 5682.
[19] A.J. Plomp, H. Vuori, A.O.I. Krause, K.P. de Jong, J.H. Bitter, Appl. Catal. A 351 (2008) 9.
[20] P. Gallezot, A. Giroir-Fendler, D. Richard, Catal. Lett. 5 (1990) 169.
[21] J. Hájek, N. Kumar, D. Francová, I. Paseka, P. Mäki-Arvela, T. Salmi, D.Yu. Murzin, Chem. Eng. Technol. 27 (2004) 1290.
[22] M. Chatterjee, Y. Ikushima, T. Yokohama, T. Suzuki, Micropor. Mesopor. Mater. 117 (2009) 201.
[23] D. Zhao, Q. Huo, J. Feng, B.F. Chmelka, G.D. Stucky, J. Am. Chem. Soc. 120 (1998) 6025.
[24] R. Mokaya, Angew. Chem., Int. Edit. Engl. 38 (1999) 2930.
[25] S. Handjani, S. Dzwigaj, J. Blanchard, E. Marceau, J.M. Krafft, M. Che, Top. Catal. 52 (2009) 334.
[26] N. Bejenaru, C. Lancelot, P. Blanchard, C. Lamonier, L. Rouleau, E. Payen, F. Dumeignil, S. Royer, Chem. Mater. 21 (2009) 522.
[27] B. Xu, T. Xiao, Z. Yan, X. Sun, J. Sloan, S.L. Gonzáles-Cortés, F. Alshahrani, M.L.H. Green, Micropor. Mesopor. Mater. 91 (2006) 293.
[28] S. Handjani, J. Blanchard, E. Marceau, P. Beaunier, M. Che, Micropor. Mesopor. Mater. 116 (2008) 14.
[29] F. Letellier, J. Blanchard, K. Fajerwerg, C. Louis, M. Breysse, D. Guillaume, D. Uzio, Catal. Lett. 110 (2006) 115.
[30] K. Hadjiivanov, H. Knözinger, M. Mihaylov, J. Phys. Chem. B 106 (2002) 2618.
[31] W. Daniell, U. Schubert, R. Glöckler, A. Meyer, K. Noweck, H. Knözinger, Appl. Catal. A 196 (2000) 247.
[32] G. Crépeau, F. Montouillout, A. Vimont, L. Mariey, T. Cseri, F. Maugé, J. Phys. Chem. B 110 (2006) 15172.
[33] C. Chizallet, P. Raybaud, ChemPhysChem 11 (2009) 105.
[34] B.L. Mojet, J.T. Miller, D.C. Koningsberger, J. Phys. Chem. B 103 (1999) 2724.

[35] C.Y. Hou, T.C. Chiu, M.H. Shih, W.J. Tsai, W.Y. Chen, C.H. Lin, J. Phys. Chem. C 114 (2010) 4502.
[36] T. Vergunst, F. Kapteijn, J.A. Moulijn, Catal. Today 66 (2001) 381.
[37] B.L. Mojet, J.T. Miller, D.E. Ramaker, D.C. Koningsberger, J. Catal. 186 (1999) 373.
[38] D.E. Ramaker, J. de Graaf, J.A.R. van Veen, D.C. Koningsberger, J. Catal. 203 (2001) 7.
[39] A.Yu. Stakheev, Y. Zhang, A.V. Ivanov, G.N. Baeva, D.E. Ramaker, D.C. Koningsberger, J. Phys. Chem. C 111 (2007) 3938.
[40] M. Che, C.O. Bennett, Adv. Catal. 36 (1989) 55.
[41] A. Giroir-Fendler, D. Richard, P. Gallezot, Catal. Lett. 5 (1990) 175.
[42] J.C. Serrano-Ruiz, A. López-Cudero, J. Solla-Gullón, A. Sepúlveda-Escribano, A. Aldaz, F. Rodríguez-Reinoso, J. Catal. 253 (2008) 159.
[43] E.V. Ramos-Fernández, J.M. Ramos-Fernández, M. Martínez-Escandell, A. Sepúlveda-Escribano, F. Rodríguez-Reinoso, Catal. Lett. 133 (2009) 267.
[44] E.V. Ramos-Fernández, A.F.P. Ferreira, A. Sepúlveda-Escribano, F. Kapteijn, F. Rodríguez-Reinoso, J. Catal. 258 (2008) 52.
[45] G. Szöllösi, B. Török, L. Baranyi, M. Bartók, J. Catal. 179 (1998) 619.
[46] G. Szöllösi, B. Török, G. Szakonyi, I. Kun, M. Bartók, Appl. Catal. A 172 (1998) 225.
[47] M. Arai, K. Usui, Y. Nishiyama, J. Chem. Soc., Chem. Commun. (1993) 1853.
[48] M. Lashdaf, J. Lahtinen, M. Lindblad, T. Venäläinen, A.O.I. Krause, Appl. Catal. A 276 (2004) 129.